Appendix 1

Model Validation

In order to validate the numerical code, 3 computations for which the analytic solution is well known were performed. Using a rigid tube, we test first, the Poiseuille solution for a constant pressure gradient and second, for an oscillatory pressure gradient. Thirdly, we use the same oscillatory pressure in an elastic tube and compare the numerical results with the Wormesley solution.

Constant pressure in a rigid tube

Model

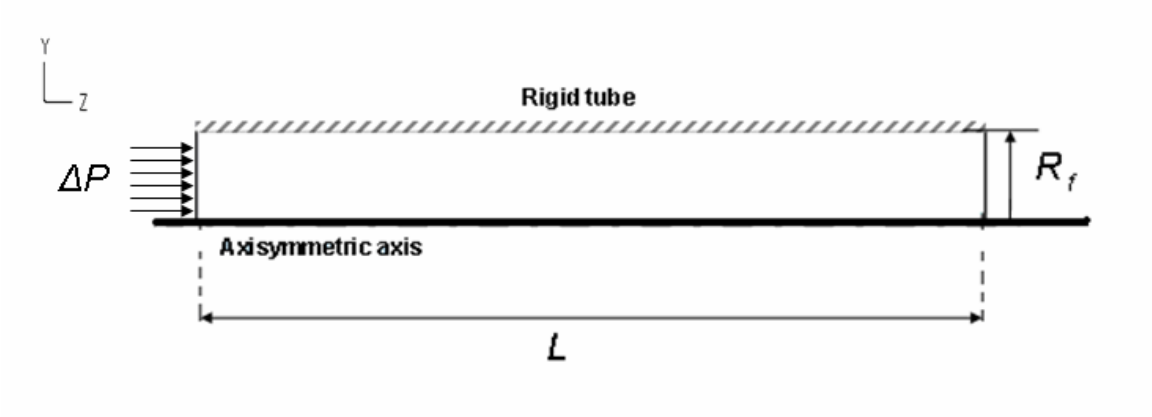

Figure. Schematic of the Poiseuille flow model. Flow in the rigid tube is driven by a pressure gradient.

Table. Characteristics of the constant pressure in a rigid tube model.

Physical parameter	Symbol	Value
Length of the pump	L	40 cm
Fluid domain radius	R_f	0.5 cm
Fluid viscosity	μ_f	0.01 g/cm s
Fluid density	ρ_f	1 g/cm^3
Pressure drop along the tube	ΔP	10 dyn/cm^2
Maximum axial velocity	$v_z^{\max}$	1.563 cm/s
Reynolds number[b]	R_e	156.3
Entry length[c]	l_e	6.254 cm

The first test case was the modelisation of a Poiseuille flow, being a constant pressure gradient in a rigid tube. The pressure gradient

$$\Delta P = P(z = L) - P(z = 0),$$

consisted in a constant normal traction applied at one extremity of the tube ($P(z = 0)$) and a zero pressure boundary condition at the other extremity of the tube ($P(z = L)$). The tube was filled with water, and was of enough length so that flow is fully developed at the end of the tube.

---

[b] The Reynolds number for the Poiseuille flow is defined as: $R_e = \frac{\rho_f v_z^{\max} D_f}{\mu_f}$ where D_f the tube's diameter ($D_f = 2 * R_f$)

[c] The entry length for the Poiseuille flow is defined as $l_e = 0.04 R_e D_f$

The numerical model consisted in 12,000 4-noded axisymmetric elements, and the time step was set to 0.005 s.

Comparison

We compared the axial velocity profile at mid length of the tube where flow is fully developed. The Poiseuille solution for the axial velocity is dependent on the pressure gradient, the fluid viscosity and the tube geometry:

$$v_z(t, y, z_o) = -\frac{\Delta P}{4\mu_f L}(y(t, z_o)^2 - R_f{}^2).$$

The error between the numerical and the analytical solutions is defined to be absolute error in axial velocity relative to the analytical solution for each point *y* along a specific cross section located at $z = z_o$ and at time t_o where flow is steady.

$$Error = \left| \frac{v_z^{num}(t_o, y, z_o) - v_z^{ana}(t_o, y, z_o)}{v_z^{ana}(t_o, y, z_o)} \right|. \qquad (*)$$

We found a very good agreement of the numerical solution with the analytical solution, and an error of about 0.09%.

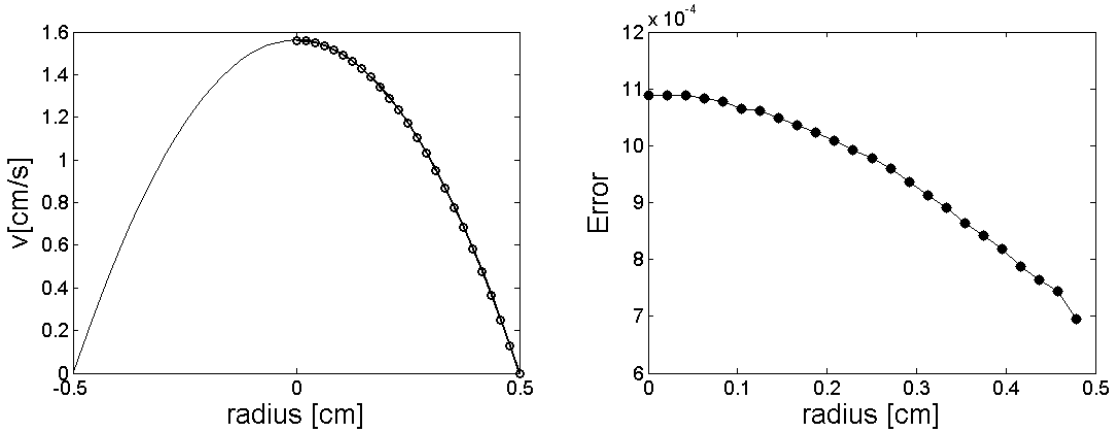

Figure. (Left) Velocity profile at a cross section located at mid-length of the tube. Analytical solution (thin line) and numerical solution (for positive Y only) (thick line and dots). (Right) Error in axial velocity between the numerical and the analytical solution along a cross section.

Pulsatile pressure in a rigid tube

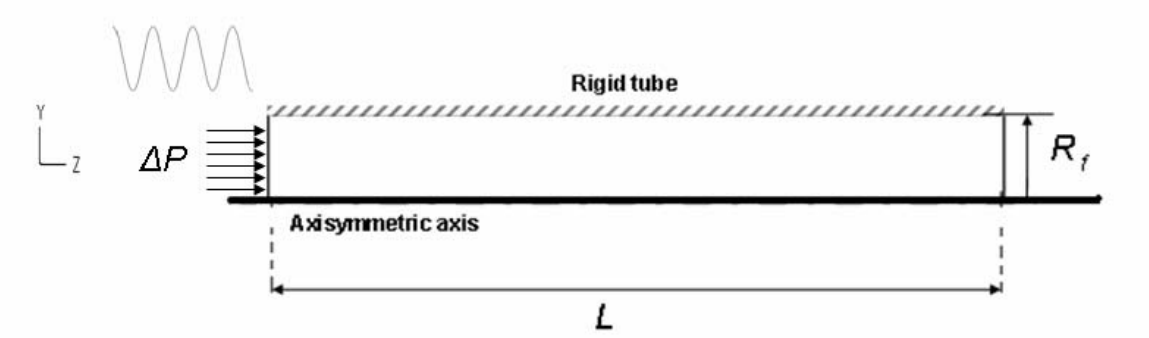

Figure. Schematic of the Poiseuille flow model with pulsatile inlet pressure.

The second test case consisted in the exact same rigid tube as the one from the previsous section with a pulsatile pressure inlet boundary condition.

$$\Delta P(t) = P\sin(\omega t),$$

with $|P| = P(z=0)$=10 dyn/cm^2 and ω=0.36 rad.s^{-1}.

The exact same numerical mesh and time step as the one from the previous section was used.

Comparison

The analytical solution is obtained by decomposing the flow into a steady and an oscillatory part. After separation of variables in the governing equation for the oscillatory part, the spatial component is found by solving a Bessel equation, and the axial velocity is expressed as: [61]

$$u_z(t, y, z_o) = \mathbf{Im}\left(i\frac{\Delta P\, {R_f}^2}{\mu_f L\Omega^2}\left(1 - \frac{J_0\left(\Lambda\frac{y(t, z_o)}{R_f}\right)}{J_0(\Lambda)}\right)\cdot e^{i\omega t}\right)$$

where J_0 is the Bessel function of order zero, and Ω a non dimensional parameter function of the material properties of the fluid, the fluid radius and the frequency of the imposed pulsatile pressure gradient:

$$\Omega = \sqrt{\frac{\rho_f \omega}{\mu_f}} R_f ,$$

and

$$\Lambda = \frac{(i-1)\Omega}{\sqrt{2}} .$$

The error between the numerical and the analytical solutions is computed using equation (*) at discrete times t_o during a period once periodic state in flow is reached.

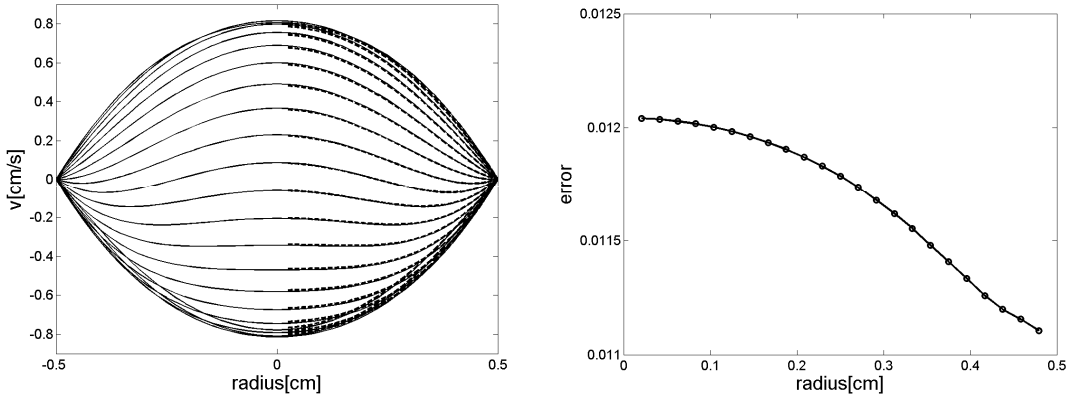

Figure. (Left) Velocity profile at a cross section located at mid-length of the tube. Analytical solution (solid line) and numerical solution (for positive Y only) (dashed line). (Right) Error in axial velocity between the numerical and the analytical solution along a cross section for different instants of a period of time.

Pulsatile pressure in an elastic tube

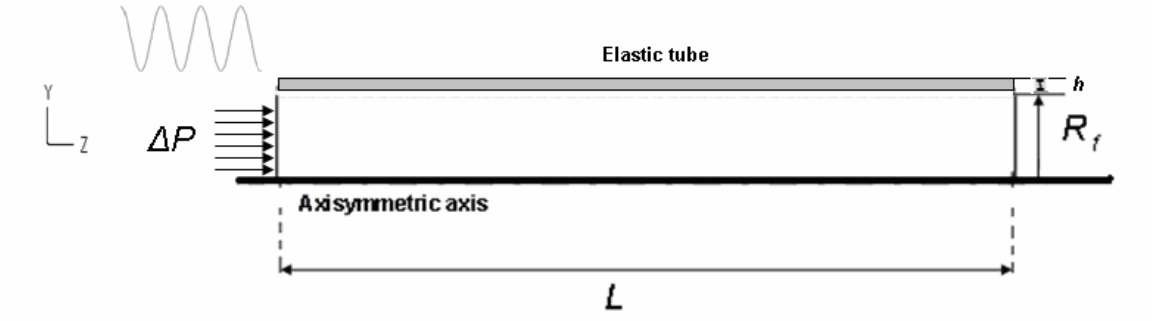

Figure. Schematic of the pulsatile pressure in an elastic tube model.

The third test case consisted in the modeling of a pulsatile flow in an elastic tube by imposing a pulsatile pressure at one extremity of the tube, the other extremity being constrained to a constant pressure of zero value. The elastic tube was modeled using a

purely linear elastic material (E_s, ν_s), and the thickness of the tube (h) was small compared to the fluid radius.

Table. Characteristics of the pulsatile flow in an elastic tube model.

Physical parameter	Symbol	Value
Length of the pump	L	40 cm
Fluid domain radius	R_f	0.5 cm
Elastic tube thickness	h	0.05 cm
Elastic tube stiffness	E_s	1 e+5 dyn/cm^2
Elastic tube Poisson's ratio	ν_s	0.3
Elastic tube density	ρ_s	1 g/cm^3
Fluid viscosity	μ_f	0.01 g/cm s
Fluid density	ρ_f	1 g/cm^3
Pressure drop along the tube	ΔP	10 dyn/cm^2

In order to avoid any wave reflection in the elastic tube, an absorbing boundary condition was used at the end of the tube ($z=L$). The absorbing boundary condition consisted on a very long elastic tube (160 cm) made out of the exact same elastic tube. At the entrance of the tube, motion of the tube in the longitudinal direction was constrained, but radial motion was allowed.

Comparison

Similarly to the case of pulsatile flow in a rigid tube, the analytical solution is obtained by decomposing the flow into a steady and an oscillatory part and coupling the Navier Stokes equations with the equations of the wall motion. The velocity in the elastic tube has an axial and a longitudinal component. After separation of variables in the governing equation for the oscillatory part, the spatial component is found by solving a Bessel equation, and the axial velocity is expressed as: [61]

$$u_z(t,y,z) = \mathbf{Im}\left(i\frac{\Delta P\, {R_f}^2}{\mu_f L\Omega^2}\left(1 - G\frac{J_0\left(\Lambda\frac{y(t,z)}{R_f}\right)}{J_0(\Lambda)}\right)\cdot e^{i\omega\left(t-\frac{z}{c}\right)}\right)$$

where c is the wave speed found by solving a quadratic equation in z where

$$z = \frac{E_s h}{(1-\nu_s^2)\rho_f R_f c^2}.$$

G is an elasticity factor given by:

$$G = \frac{2+\varsigma(2\nu_s - 1)}{\varsigma(2\nu_s - g)},$$

where

$$\varsigma = \frac{E_s h}{(1-\nu_s^2)\rho_s R_f c^2},$$

and

$$g = \frac{2J_1(\Lambda)}{\Lambda J_0(\Lambda)}.$$

The error between the numerical and the analytical solutions is computed using equation * at discrete times t_o during a period once periodic state in flow is reached.

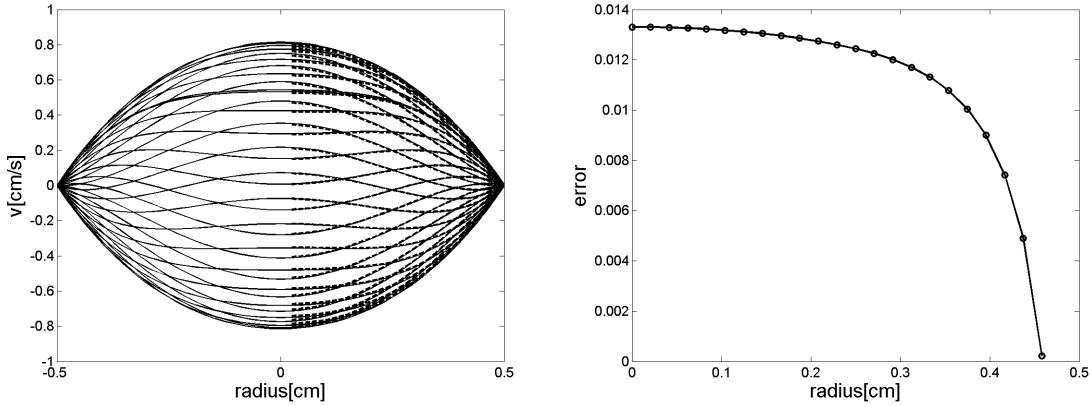

Figure. (Left) Velocity profile at a cross section located at mid-length of the tube. Analytical solution (solid line) and numerical solution (for positive Y only) (dashed line). (Right) Error in axial velocity between the numerical and the analytical solution along a cross section for different instants of a period of time.

Appendix 2

Wave dynamics

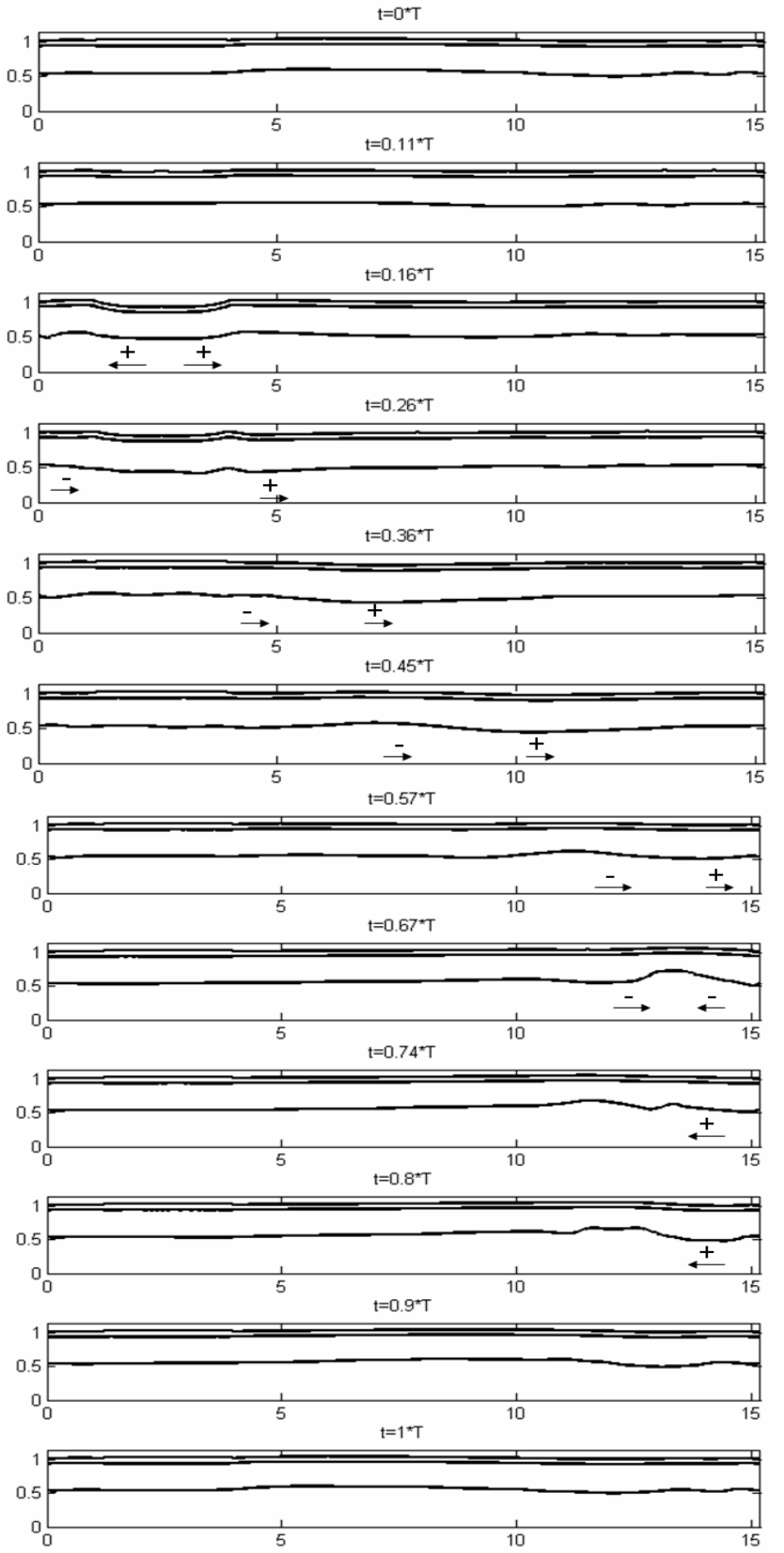
t=0*T
t=0.11*T
t=0.16*T
t=0.26*T
t=0.36*T
t=0.45*T
t=0.57*T
t=0.67*T
t=0.74*T
t=0.8*T
t=0.9*T
t=1*T
0
0.5
1
5
10
15
+
-

Figure (a)

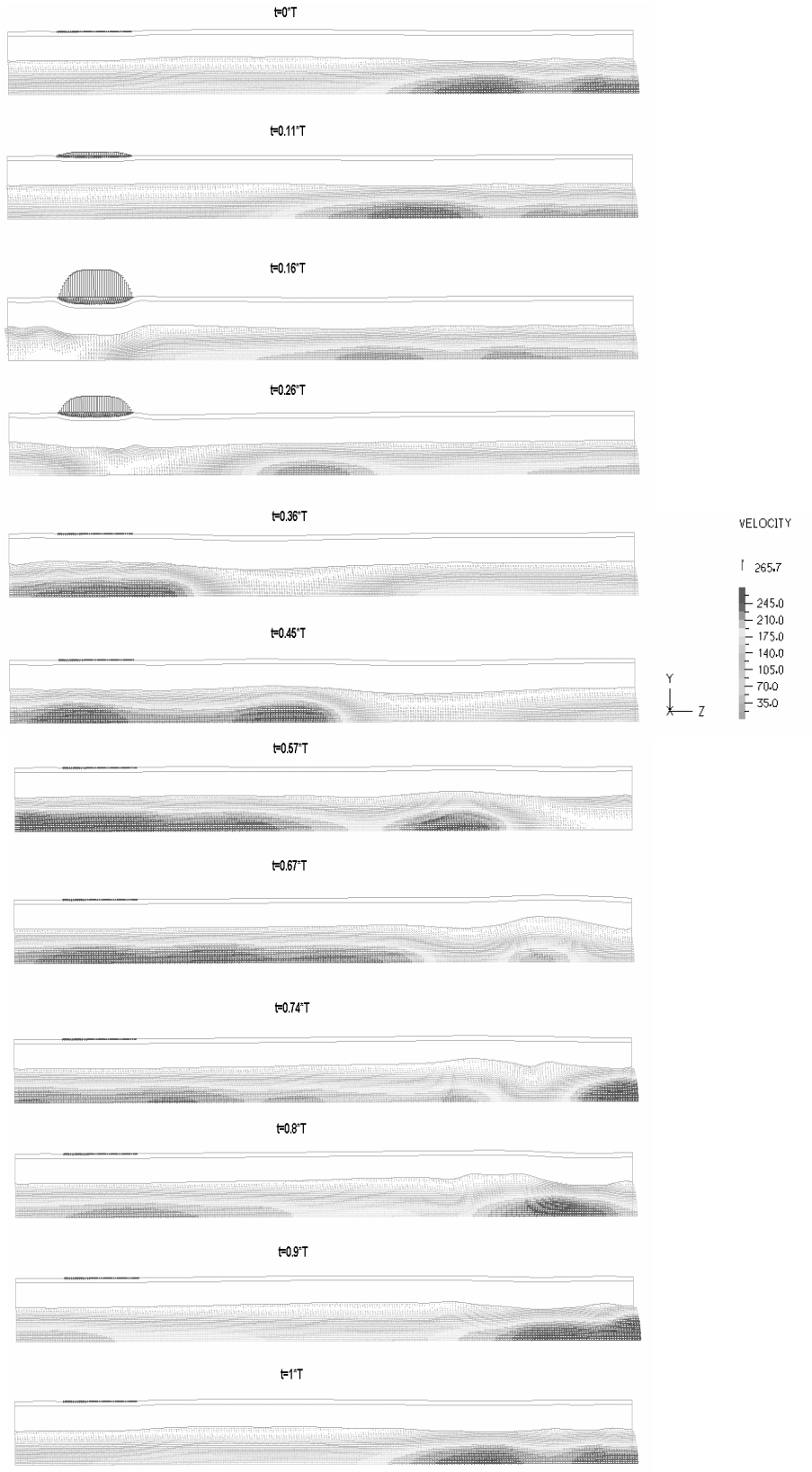
t=0*T
t=0.11*T
t=0.16*T
t=0.26*T
t=0.36*T
t=0.45*T
t=0.57*T
t=0.67*T
t=0.74*T
t=0.8*T
t=0.9*T
t=1*T
VELOCITY
265.7
245.0
210.0
175.0
140.0
105.0
70.0
35.0
Y
X
Z

Figure (b)

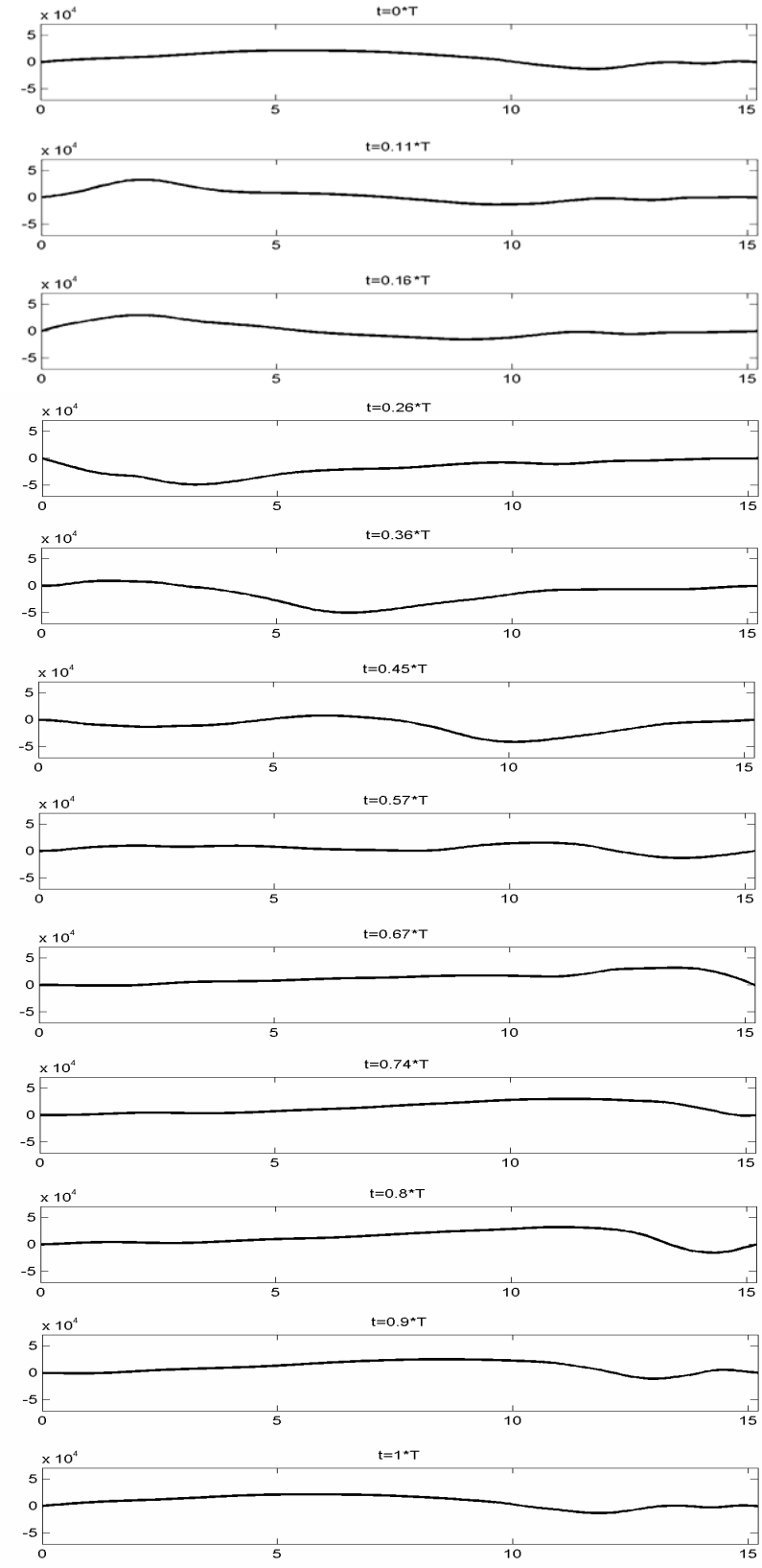
t=0*T
t=0.11*T
t=0.16*T
t=0.26*T
t=0.36*T
t=0.45*T
t=0.57*T
t=0.67*T
t=0.74*T
t=0.8*T
t=0.9*T
t=1*T
x 10^4
5
0
-5
0
5
10
15

Figure (c)

Figure. Illustration of the propagating waves in the multilayer impedance pump. Example for f=10.1 Hz. (a) Selected frames of the model outline over one period of time at periodic conditions. The time t of each selected frame is expressed as a fraction of the period T. (b) Corresponding snapshots of the axial velocity fluid field for each of the selected times (c) Axial pressure longitudinal distribution for each of the selected times.

Appendix 3

MIP with a viscoelastic material

A model of MIP using a viscoelastic gelatin that is time dependant and temperature independent has been implemented. The MIP model is identical to the one described in section 2.1.

The stiffness, Poisson's ratio and density of the gelatin, are the same as in section 2.1 (see table). The gelatin being treated as a viscoelastic material, the state of stress in the gelatin follows:

$$s_{ij}(t) = 2G_{gel}(0)e_{ij}(t) + 2\int_0^t e_{ij}(t-\tau)\frac{dG_{gel}(\tau)}{d\tau}d\tau,$$

$$\sigma_{ij}(t) = 3K_{gel}(0)e_{kk}(t) + 3\int_0^t \varepsilon_{kk}(t-\tau)\frac{dK_{gel}(\tau)}{d\tau}d\tau,$$

where t is the time,

$$s_{ij} = \sigma_{ij} + \frac{1}{3}\delta_{ij}\sigma_{kk},$$

is the deviatoric stress, δ_{ij} is the Kronecker delta, σ_{ij} is the stress,

$$e_{ij} = \varepsilon_{ij} - \frac{1}{3}\delta_{ij}\varepsilon_{kk},$$

is the deviatoric strain, ε_{ij} is the strain, $G_{gel}(t)$ is the shear modulus and $K_{gel}(t)$ is the bulk modulus defined by:

$$G_{gel}(t) = \frac{E_{gel}(t)}{2(1+\nu_{gel})},$$

$$K_{gel}(t) = \frac{E_{gel}(t)}{3(1-2\nu_{gel})}.$$

In the viscoelastic formulation, the shear and bulk moduli are expressed in terms of a Prony-Dirichlet series where variation of temperature is neglected.

$$G_{gel}(t) = G_{gel}(0) + G_o e^{-d_1 t},$$

$$K_{gel}(t) = K_{gel}(0) + K_o e^{-d_2 t},$$

where $G_{gel}(0)$ is the final shear modulus, $K_{gel}(0)$ the final bulk modulus, G_o and K_o are constant coefficients, and d_1 and d_2 are the relaxations parameters for the shear and bulk modulus respectively.

Table. Characteristics of viscoelastic gelatin.

Physical parameter	Symbol	Value
Stiffness	E_{gel}	5 e+4 dyn/cm^2
Poisson's ratio	ν_{gel}	0.49
Density	ρ_{gel}	1 g/cm^3
Shear modulus	G_{gel}	8.3 e+5 dyn/cm^2
Bulk modulus	K_{gel}	1.67 e+4 dyn/cm^2
Shear coefficient	G_o	8.3 e+5
Bulk coefficient	K_o	1.67 e+4
Shear relaxation parameter	d_1	1,000
Bulk relaxation parameter	d_2	1,000

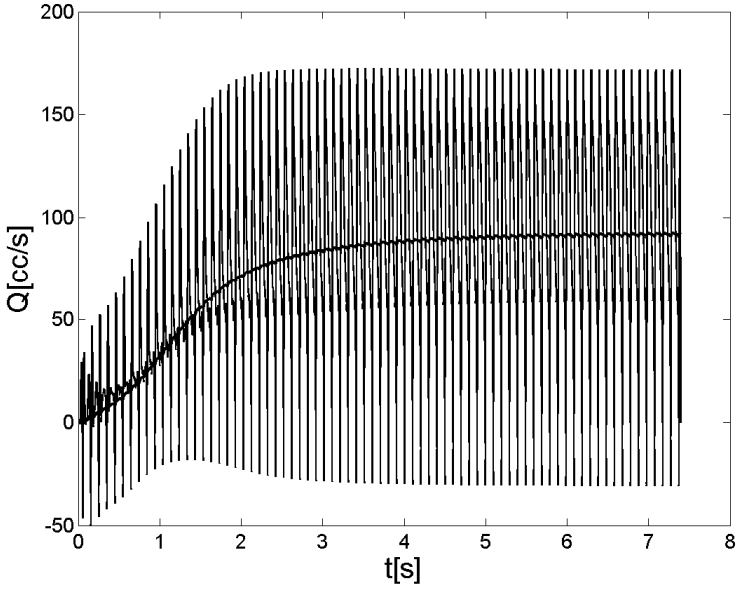

Figure. Exit flow rate time history for the MIP using a viscoelastic gelatin layer. Frequency of excitation is 10.1 Hz. Mean exit flow reaches 90.6 cc/s.

This viscoelastic MIP model demonstrates that the MIP exhibits the same behavior when a viscoelastic material is used to represent the gelatin. Results show that the nonlinearities introduced by the viscoelastic material can be beneficent to the pumping if appropriate material properties are chosen.

Appendix 4

Error in linearization

Analytical

The error in solving for small strains can be estimated by calculating the error in strain linearization for the maximum strain observed (30%):

$$\varepsilon_{ij} = \frac{1}{2}\left(u_{i,j} + u_{j,i} - u_{k,i}\cdot u_{k,j}\right) = \frac{1}{2}\left(u_{i,j} + u_{j,i}\right) - \underbrace{\frac{u_{k,i}\cdot u_{k,j}}{2}}_{error}$$

$$error = ½* (0.3)^2 = 0.045 < 5\%$$

Numerical

In addition, we performed a comparison between two numerical simulations of the MIP, one with the small strain assumption and one with the large strain assumption for the pump excited at 11.5 Hz. We found a relative error in exit flow rate of 4.6104 e-4 (less than 0.05%), which confirms the analytical results.

$$error = \underset{t\in[t_o,t_o+T]}{mean}\left(\frac{Q^{small\ strain}(t,z_o) - Q^{large\ strain}(t,z_o)}{Q^{small\ strain}(t,z_o)}\right)$$

Appendix 5

High frequency results

The MIP defined in section 6.2.2 was excited at 5% of its external radius (instead of the 10% from the original MIP model) and frequencies ranging from 30 to 45 Hz.

Impulse response

The same impulse excitation as the one described in section 3.2 was applied to the MIP model excited at 5% of its external radius. The spectrum of the exit flow rate is similar to the one described in section 3.2, confirming the invariance of the model's natural frequencies with respect to pinching amplitudes.

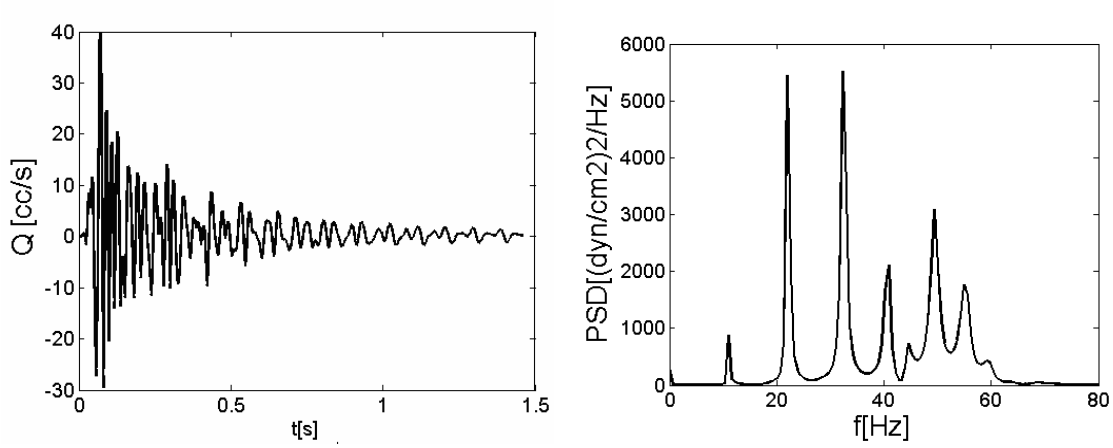

Figure. Impulse response of the MIP model excited at 5% of its external radius. (Left) Exit flow rate variation in time under triangular impulse excitation. (Right) The associated Power Spectrum Density (PSD).

Exit flow rate and frequency of excitation

The mean exit flow rate ($\overline{Q}$) is calculated for frequencies of excitation ranging from 30Hz to 45Hz. It is found positive and seem not to have a specific correlation with the natural frequencies exhibited by the spectrum analysis. Although the excitation amplitude is only 5% of the external radius, flow reaches up to 50 cc/s.

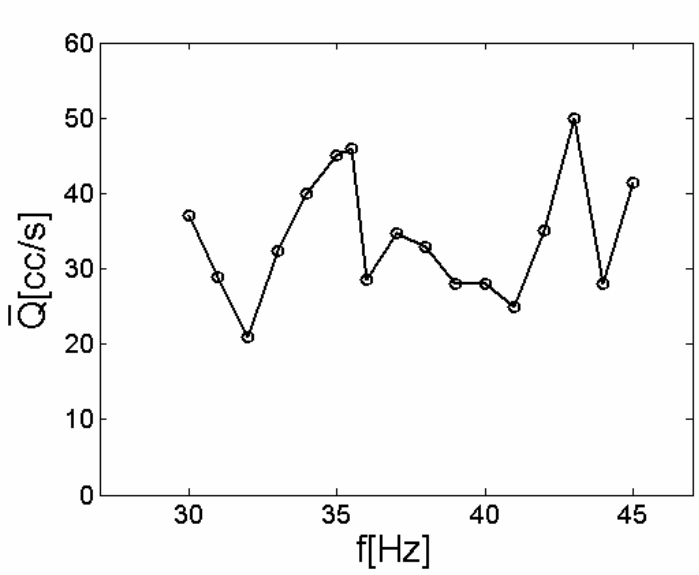

Figure. Mean exit flow rate ($\overline{Q}$) as a function of the excitation frequency (*f*).

Wall displacement, axial pressure longitudinal distribution & axial velocity longitudinal distribution

The wall displacement, axial pressure longitudinal distribution and axial velocity longitudinal distribution is plotted over a period of time once periodicity in the flow is achieved.

f	Wall position	Axial pressure	Axial velocity
30Hz	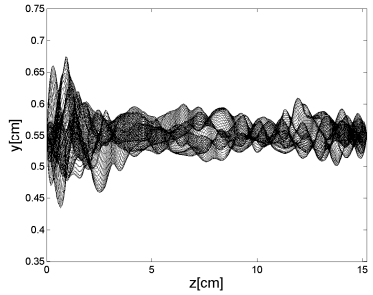	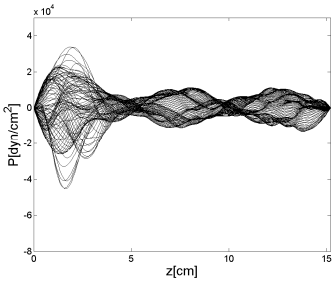	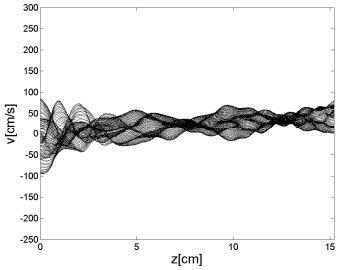
31Hz	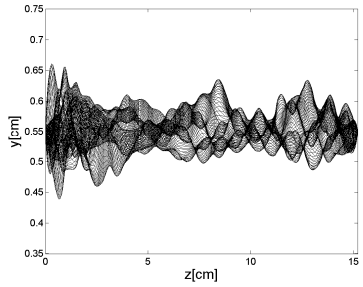	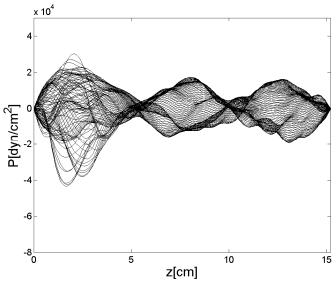	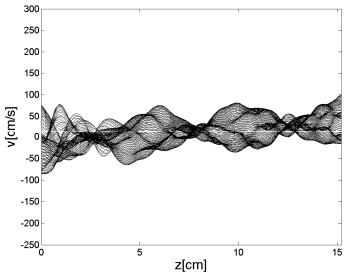
32Hz	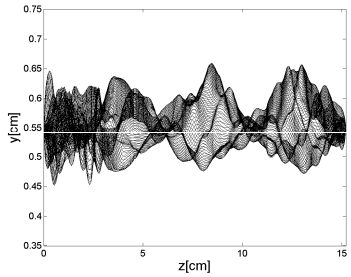	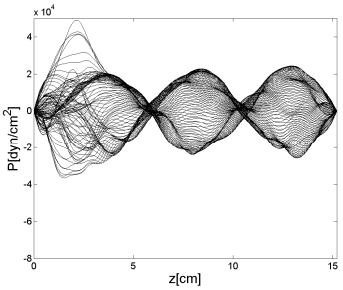	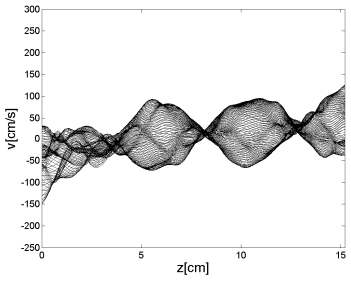
33Hz	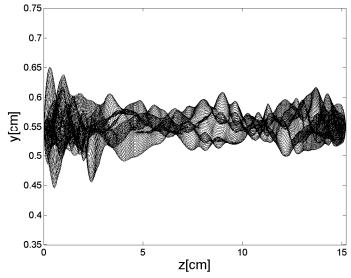	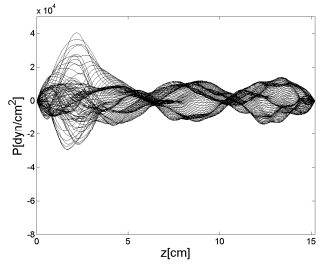	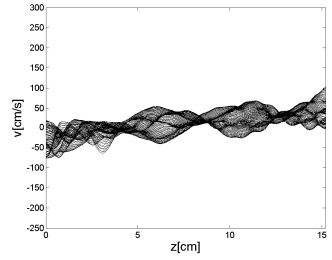

34Hz

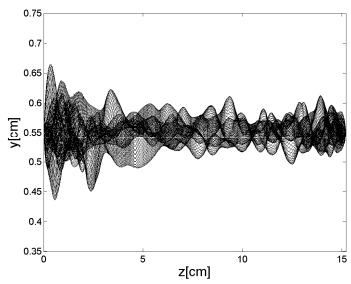

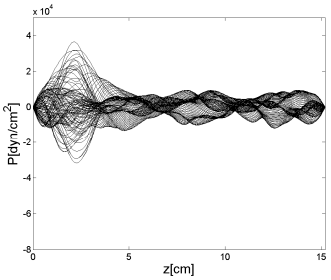

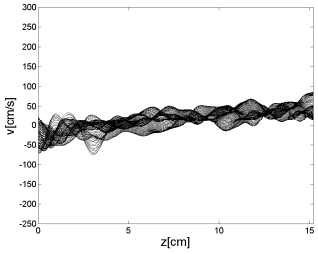

35Hz

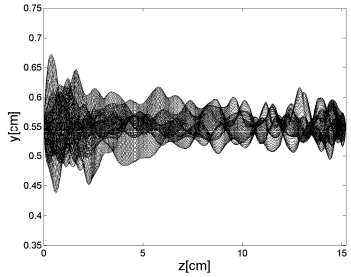

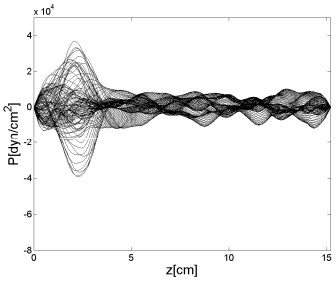

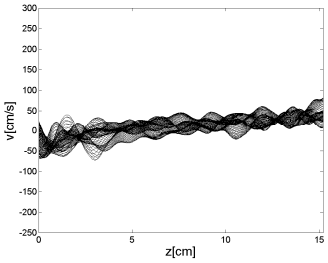

36Hz

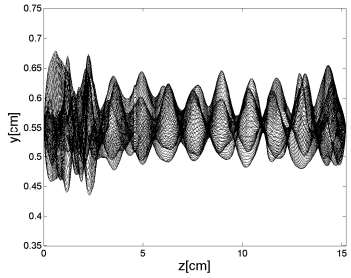

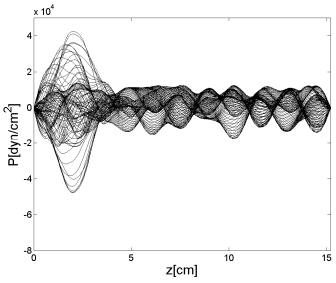

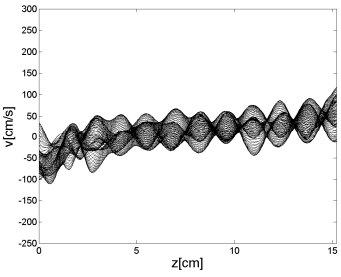

37Hz

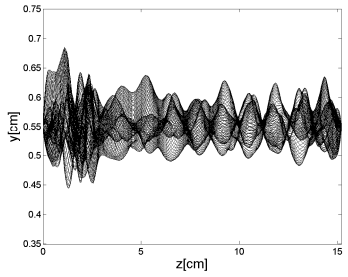

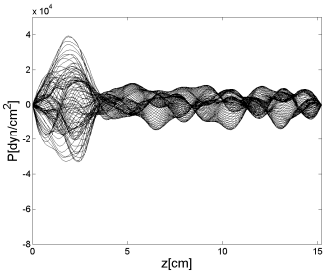

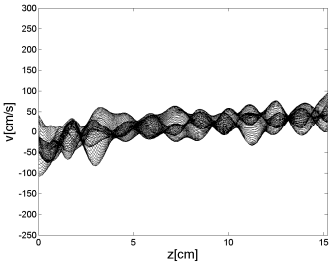

38Hz

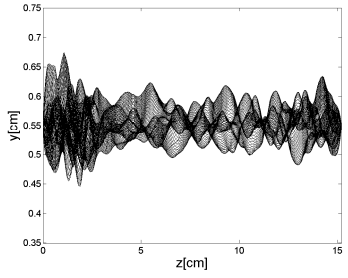

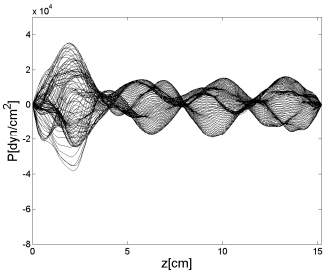

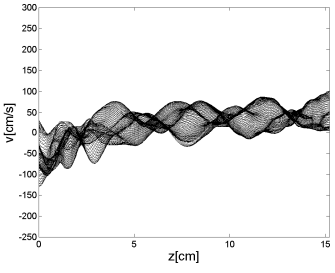

39Hz

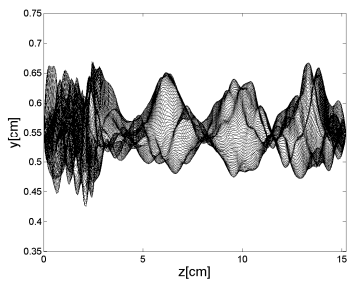

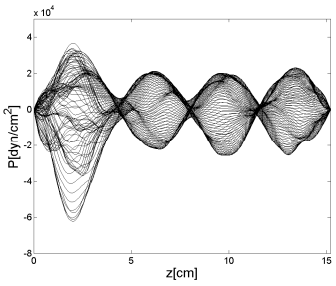

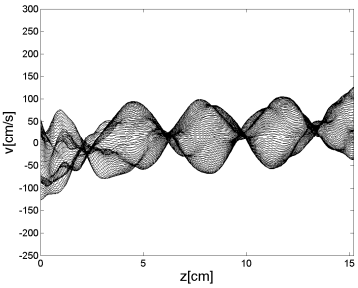

40Hz

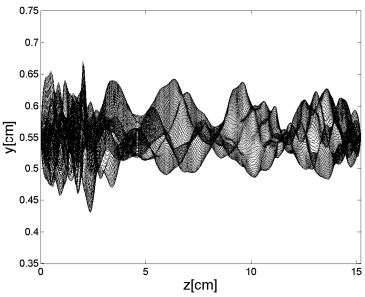

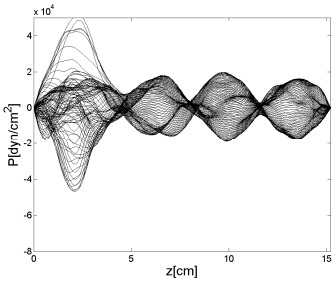

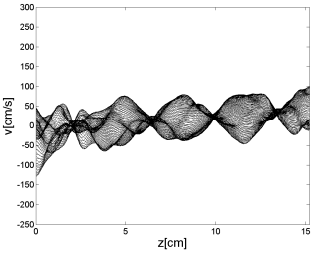

41Hz

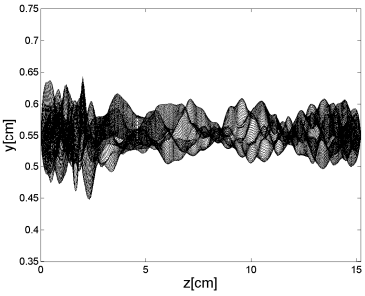

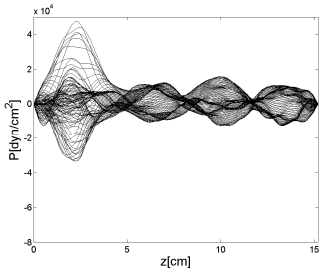

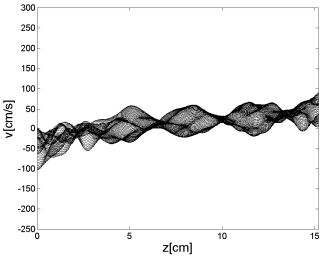

42Hz

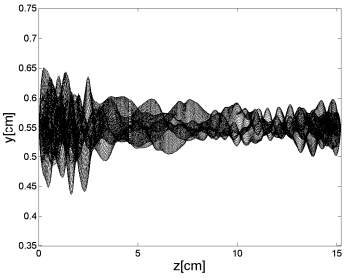

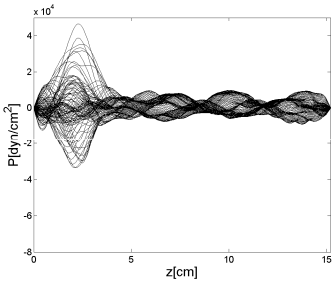

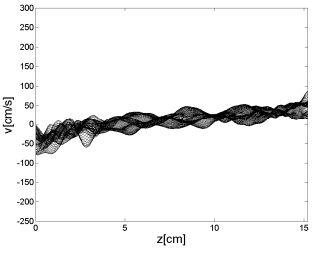

43Hz

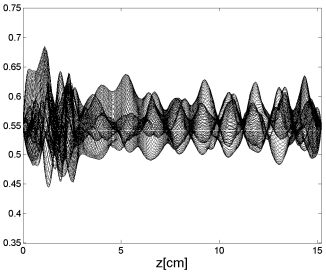

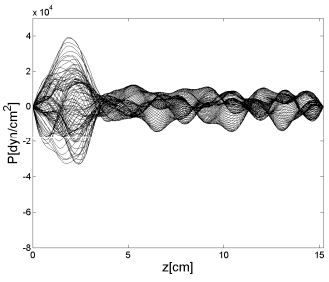

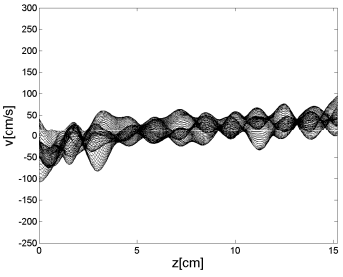

44Hz

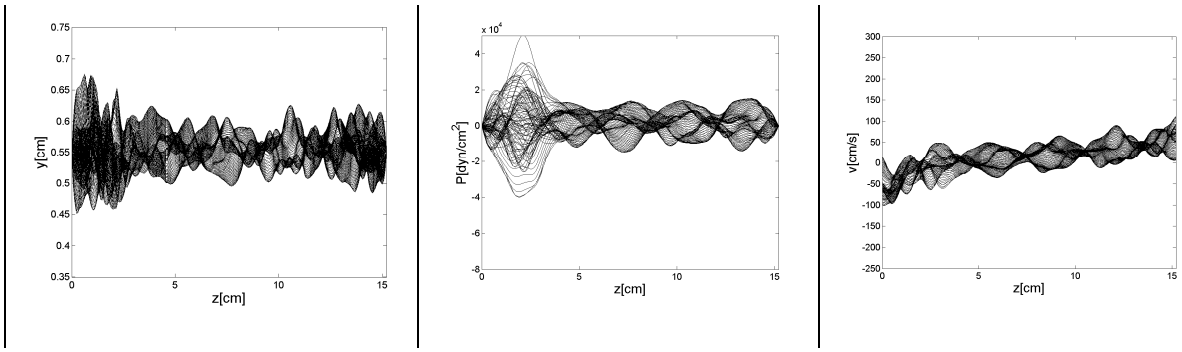

Figure. Wall displacement, axial pressure longitudinal distribution and axial velocity longitudinal distribution over a period of time once periodicity in the flow is achieved.

Appendix 6

Viscous diffusion time

We estimate the diffusion time for the entire flow to be affected by the wall motion by using the impulsively actuated oscillatory wall (2nd Stokes problem).

Considering an impulsively oscillatory wall in the Z direction of velocity *U* and of frequency *f*, the velocity *u* in the fluid can be expressed using the self-similar variable η:

$$u = U\, e^{-\eta}\, \mathbf{cos}\left(2\pi f t - \eta\right), \qquad \eta = y\sqrt{\frac{\pi}{\nu t}}.$$

The fluid at the distance $y=d$ away from the moving wall will have 0.99 of the wall velocity (U) when :

$$\eta = -\mathbf{ln}\left(\frac{u}{U}\right) \Rightarrow d\sqrt{\frac{\pi}{\nu t^*}} = 0.0101.$$

The time t^* to reach 99% of the wall velocity at the axis of symmetry of the pump model (d=0.55cm) is then:

$$t^* = \frac{\pi}{\nu}\left(\frac{d}{0.0101}\right)^2 \approx 2.6\mathrm{e}+5\mathrm{s} \approx 74\mathrm{h}.$$